Pressure responses and phase transitions during the release of high pressure CO_2 from a large-scale pipeline

Xiaolu Guo [a], Xingqing Yan [a], Jianliang Yu [a†], Yang Yang [a], Yongchun Zhang [b], Shaoyun Chen [b], Haroun Mahgerefteh [c], Sergey Martynov [c], Alexander Collard [c]

[a] School of Chemical Machinery and Safety,
Dalian University of Technology, Dalian, 116024,China

[b] School of Chemical Engineering,
Dalian University of Technology, Dalian, 116024, China

[c] Department of Chemical Engineering,
University College London, London WC1E 7JE, UK

[†]Corresponding Author
School of Chemical Machinery and Safety
Dalian University of Technology
No 2 Ling Gong Road
Dalian, 116024,China
e-mail: yujianliang@dlut.edu.cn
Tel.: +86 411 84986281
Fax: +86 13998576027

Revised manuscript submitted to *Energy*

June, 2016

Pressure responses and phase transitions during the release of high pressure CO_2 from a large-scale pipeline

Xiaolu Guo [a], Xingqing Yan [a], Jianliang Yu [a†], Yang Yang [a], Yongchun Zhang [b], Shaoyun Chen [b], Haroun Mahgerefteh [c], Sergey Martynov [c], Alexander Collard [c]

Abstract

As part of the Carbon Capture and Storage (CCS) process, pipeline transportation is the safest and most economic option for delivering captured CO_2 to a storage site. However, in the event of pipeline rupture an enormous mass of CO_2 may be released very rapidly, presenting several risks to the pipeline and surrounding population including the significantly increased risk of brittle fracture in the pipe wall. The study of pressure variation and phase change in CO_2 during pipeline blowdown can contribute to the understanding of fracture initiation and propagation, as well as downstream CO_2 diffusion behavior. As part of the CO_2QUEST project, a reusable, industrial scale pipeline experimental apparatus with a total length of 258 m and the inner diameter of 233 mm was fabricated to study pure CO_2 pipeline blowdown. A dual-disc blasting device was used to remotely control the opening of the pipeline. The instantaneous pressure response following release was measured with high frequency pressure transducers. Variation in fluid temperature at the top and bottom of pipeline was also recorded. Six groups of pure CO_2 pipeline release experiments were conducted with initially gaseous and dense phase inventories with three orifice diameters (15 mm, 50 mm and Full Bore Rupture). The pressure undershoots, rebounds and quasi static pressures were observed during the release as result of the propagation of a series of expansion waves. The process of pressure drop and rebound was accompanied by the occurrence of gas-liquid two-phase flow. The complicated phase transitions were obtained during depressurization of gaseous and dense CO_2 releases.

Keyword: CO_2 release, Pressure response, Phase transition, Large-scale pipeline blowdown.

1 Introduction

Following the Copenhagen Climate Change Conference (2009) there is a broad political consensus to limit the rise in global temperatures to 2 °C above pre-industrial levels. This requires a 50-80 % reduction in CO_2 emissions by 2050 [1]. Carbon Capture and Storage (CCS) is a process by which waste CO_2 is captured from large emitters and stored underground, thus reducing direct emissions to the atmosphere and mitigating the environmental impact of fossil fuels [2].

As a part of the CCS chain, pipeline transportation of CO_2 from emitter to storage site is considered the safest and most efficient transportation option [3]. The large scale implementation of CCS will require large transportation networks, potentially between 95,000 and 550,000 km of CO_2 pipelines by 2050 [4]. Safety issues surrounding the operation of CO_2 pipelines are expected to be complex compared to current practice [5,6]. Additionally, CO_2 transmission pipelines may be expected to suffer from accidental releases caused by defects such as mechanical damage, corrosion, construction or material defects, soil movement or even operational mistakes in a similar fashion to hydrocarbon pipelines, for example [7].

Understanding the processes occurring inside a CO_2 pipeline during outflow is essential to investigating fracture propagation and atmospheric dispersion of the inventory [8-12]. For an initially high pressure inventory, whether gaseous, dense phase or supercritical, there is likely to be a complex phase-transition as CO_2 decompresses during pipeline blowdown [13]. The rupture of a CO_2 pipeline will result in a series of expansion waves that propagate into the undisturbed fluid in the pipe. Significant Joule-Thomson cooling associated with the rapid

expansion of the inventory can result in very low and potentially harmful temperatures in the fluid and pipe wall [14]. The precise tracking of these expansion waves and temperature variations, and their propagation as a function of time and distance along the pipeline, is necessary to predict a pipeline's propensity to fracture [15]. A pipeline failure (most commonly a puncture) may escalate to a fracture if the force acting on the defect overcomes the fracture toughness of the wall material. The fracture may be either in the ductile or brittle regime depending on the nature of the rupture [16].

In order to develop accurate models for predicting the depressurization and phase transition behavior during CO_2 pipeline blowdown, several experimental research programs have been performed. Cosham et al. [17] reported three West Jefferson Tests conducted on behalf of National Grid at the Spadeadam Test Site to investigate ductile fracture propagation in pipelines transporting liquid or dense phase CO_2. The depressurization of liquid or dense phase CO_2 after a rupture was characterised by a rapid depressurization through the liquid phase, and then a long plateau. Clausen et al. [18] described the results of depressurizing during CO_2 venting with an onshore 50 km long, 24 inch diameter buried pipeline from initially supercritical conditions. Pressure and temperature were measured at the two ends of the pipeline. According to experimental data at the first end location two-phase behavior was observed upstream the release for the first 2,5 hours and there was no indication of dry ice formation upstream the two release points. Cosham et al. [19] performed a program of shock tube tests with CO_2 and CO_2-rich mixtures in order to study depressurization behavior in the gaseous and dense phases. The researchers found that the plateau in the depressurization curve of dense CO_2 and CO_2-rich mixtures was longer than that of natural gas, gaseous CO_2

and gaseous CO_2-rich mixtures. Li et al. [20] developed a 23 m long circulation pipeline system with a 30 mm inner diameter to study the leakage behavior of high pressure CO_2 flow. The pressure decrease in the pipeline was much larger for supercritical leakage due to the higher density than that of the gas-phase. Huh et al. [21] studied the severe pressure and temperature drops during the depressurization of dense CO_2 in a 51.96 m long test tube with an inner diameter of 3.86 mm. It was found that the initial pressure drop was well estimated by OLGA for both pure CO_2 and mixtures, but the numerical simulation did not provide reliable temperature drop predictions. Koeijera et al. [22,23] built a horizontal pipeline with a length of 139 m and an inner diameter of 10 mm in order to study the depressurization behavior of liquid CO_2. The results showed that the pressure dropped rapidly at first and then levelled off. The rarefaction wave travelled along the length of the tube and was reflected at the closed end. DNV-GL [24] carried out the liquid CO_2 depressurization experiments using a 30 m long, 2 inch diameter stainless steel tube. The pressure and temperature evolution during blowdown was defined by the balance between mass leaving the system, internal processes such as liquid and vapor expansion, phase change and heat supplied by the surroundings. The COSHER joint industry project [25] employed a 226.6 m long pipeline loop formed from 219.1 mm diameter steel pipe and fed from both ends by a 148 m^3 reservoir of CO_2 to study pipeline depressurization and dispersion of initially dense phase CO_2. A fast pressure drop to saturation conditions during CO_2 release was observed after rupture. The minimum fluid temperature recorded was $-17.8\ ^{\circ}C$ in the reservoir and $-78\ ^{\circ}C$ in the 219.1 mm pipeline loop.

This paper presents the results of pipeline blowdown experiments using a 258 m long, 233 mm inner diameter pipeline containing CO_2 at various initial conditions. Fluid pressures and temperatures in the pipeline were recorded. The experiments' main objective was to improve the understanding of depressurization behavior and phase transition during the release of CO_2.

2 Experiments

2.1 Experimental setup

The main components of the experimental setup are shown in Fig.1. The apparatus consisted of a single pipeline with a length of 257 m and inner and outer diameters of 233 and 273 mm respectively, a dual-disc blasting pipe with a length of 1 m, two CO_2 injection lines, a heating system and two data measurement systems. The main pipe was made of 16MnR steel, which had a minimum allowable temperature of -40 °C, whereas the dual-disc blasting pipe was made of grade 304 stainless steel and its minimum allowable temperature was -196 °C. The pipeline apparatus was designed to operate at a maximum pressure of 16 MPa. 24 concrete column foundations were built to support the pipeline at a height of 1.3 m above ground.

The inventory temperature could be maintained or increased during charging or before experiments using a heating system made up of heating tape and a 50 mm thick thermal insulation layer mounted on the outer pipe surface, the tape was controlled via six temperature controllers. The heating tape power was 50 kW. The heating system was designed to vary the initial temperature of the inventory from 0 to 40 °C.

To open the pipeline and initiate experiments a dual disc blasting device is used. This device is 1 m long and consists of two rupture discs and two disc holders, a solenoid valve and two pipe sections (Section 1 with a length of 0.6 m; Section 2 with a length of 0.3 m) connected by a flange and bolts. A schematic of the dual-disc blasting device is shown in Fig. 2. The pipeline was charged with the appropriate mass of inventory for each experiment and the heating coils used to achieve the desired initial conditions. The pressure P_2 in section I was maintained proportionally to the pressure P_1 inside the main pipeline. To initiate the experiment, the pressure P_2 in section I was rapidly raised, forcing the disc B to break, resulting in the near simultaneous rupture of disc A. Because the length of the dual-disc device (1 m) is much shorter than the main pipeline (257 m), its influence on pressure and temperature measurements in the main pipe can be ignored.

The recoil-shock created when initiating full bore rupture (FBR) experiments was significant. A reinforced anchor device was designed and installed to hold the release end of the pipeline firmly in place, as shown in Fig. 3. The device consisted of steel frames, steel plate, and anchor bolts anchored firmly to the concrete foundation. The reacting force and frictional force of the reinforcement device could resist an acting force of more than 400 kN.

2.2 Pipeline instrumentation

Various instruments were installed along the pipeline, including 4 low frequency pressure sensors, 8 high frequency pressure sensors, 18 thermocouples on the upper half of pipeline, 6 thermocouples on the bottom half of pipeline and 12 thermocouples on the outer wall of pipeline. Pressure change in the overall process was measured using PPM-S322G pressure transducers with a frequency response of 1 kHz and an accuracy of 0.25 %FS of full scale.

Pressure change at the beginning of release was measured using PPM-S116B-0EM pressure transducers with a frequency response of 100 kHz and an accuracy of 0.25 %FS of full scale. Temperature was measured using K-type thermocouples which had a response time of 100 ms and a range of -200 °C to 1300 °C, and uncertainty of ±1 °C. The installing angle of measurement points are shown in Fig. 4.

Data was recorded using two independent measuring systems, an NI cRIO-9025 system which was used to simultaneously sample 4 low frequency pressure sensors and all the thermocouples and an NI cDAQ-9188 system which was used to sample 8 high frequency pressure sensors. The NI cRIO-9025 system consisted of one 9025, four 9144 chasses and twelve 9219 modules for temperature and pressure signal acquisition. The 5 chasses were connected using ordinary internet access cable. The communication protocol used EtherCAT at 110 ms/sample to ensure synchronised data gathering. All of the data acquired would be cached in the host 9025. The NI cDAQ-9188 system consisted of two 9188 of 4 channels with a high-speed of 500 kS/s. LabVIEW software was used to transfer the data from the 9025 or 9188 to a local computer by Ethernet.

2.3 Experiments conducted

In this paper, six groups of pure CO_2 release experiments were performed to investigate depressurization behavior and phase transition during the release of CO_2 from a pipeline. Each group used initially vapor or dense phase CO_2. Three different orifice diameters were also used for each group of tests (15 mm, 50 mm and Full Bore Rupture). Thus six experiments in total were conducted. The initial experimental conditions of the six tests are presented in Table 1.

Table 2 reports the instruments from which data is available for the listed experiments, including instrument type, number and location.

3 Experimental results

In this section the results of six release experiments with three different orifice sizes (15 mm, 50 mm and FBR) are described and the recorded pressure response and phase transition data are analyzed. In all the following figures a rightward pointing arrow ("→") indicates decompression wave propagation from the discharge end to the closed end of the pipe, while a leftward pointing arrow ("←") indicates decompression wave propagation from the closed end to the discharge end. The numbers above the arrows represent the times for the decompression wave to travel the length of the pipe and their propagation velocities in the 1st and 2nd periods. Three kinds of pressure response parameters are defined as follows: (1) The pressure drop amplitude (ΔP_d) is the difference between the maximum pressure in front of the decompression wave and the minimum pressure behind the decompression wave (2). The pressure rebound amplitude (ΔP_r) is the difference between the minimum pressure behind the decompression wave and the recovery pressure following depressurization (3). The quasi-static pressure (P_{qs}) is the recovery pressure following depressurization. P_1, P_2, P_3, P_4, P_5, P_6, P_7, P_8 and P_9 in all figures indicate the pressures at different locations along the pipe.

3.1 Gas phase tests

3.1.1 Pressure response

Fig. 5 shows the evolution of fluid pressure after rupture for tests 1, 2 and 3. The total depressurization times for each experiment are 1946 s, 159 s and 15 s respectively. It may be

observed for tests 1 and 2 that the pressure gradient along the length of the pipe is small during depressurization, this is not the case for test 3.

In the magnified regions of Fig. 5(a) and (b), the pressure response processes recorded by P_2, P_5, P_7 and P_9 at the beginning of tests 1 and 2 are presented. In the 1st period of tests 1 and 2 the decompression wave propagates from the orifice to the closed end at the local speed of sound in the inventory. Behind the decompression wave the inventory pressure drops rapidly. Following the pressure undershoot droplet formation and gasification causes the pressure to recover almost to the initial P_{qs} in both tests. ΔP_d and ΔP_r reduce greatly with the increase in distance from the measured point to the orifice. In the 2nd period of tests 1 and 2 the reflected decompression wave travels from the closed end of the pipe towards the rupture end, causing a further decrease in pressure from P_9 to P_2 in turn. The inventory achieves a second P_{qs}. ΔP_d and ΔP_r are fractionally greater with increasing distance from the orifice and the value of P_{qs} nearer the orifice was affected by the decompression wave and was below the overall P_{qs}. On the whole, with the decompression wave reflecting repeatedly, ΔP_d, ΔP_r and P_{qs} reduced gradually until the pressure drop and rebound inside the pipeline were no longer obvious. Comparing the pressure response parameters of tests 1 and 2, ΔP_d of the two were very close, but ΔP_r of test 2 (50 mm orifice) was smaller than that of test 1 (15 mm orifice). P_{qs} of tests 1 and 2 reduced about 0.01 MPa and 0.11 MPa respectively following each passage of the decompression wave.

Fig. 5 (c) shows the variation of fluid pressure with time for test 3. After rupture, the decompression wave propagates with an initial speed of 242.43 m/s. The intersection of curve 1 with the pressure histories indicates the times at which droplets form at each location in the

gaseous inventory. ΔP_d from P_2 to P_9 decreased from 1.79 MPa to 0.62 MPa successively. After droplets formed the rate of pressure loss in the pipe decreased to about 2.47 MPa/s. The passage of the reflected decompression wave past each transducer, indicated by the intersection of the pressure histories with curve 2, caused an increase in the rate of recorded pressure drop.

Fig. 6 shows the rate of pressure change with time in 1st period of tests 1, 2 and 3. For tests 1 and 2, after undershoot the pressure change rates at P_2, P_5, P_7 and P_9 sharply increased to maximum values and soon returned to zero. This phenomenon is caused by droplet gasification. The minimum and maximum values of the pressure change rates decreased successively with increasing distance from the orifice. For P_2, P_5, P_7 and P_9, the amplitude of the pressure rise rate was much larger than the pressure drop rate and the duration time of the pressure rise was shorter than that of the pressure drop. Comparing the pressure change rates of tests 1 and 2, the minimum value of test 1 was smaller than that of test 2, and the maximum value of test 1 was much greater than that of test 2. For test 3, as there was no pressure rebound, the pressure change rate at P_2, P_5, P_7 and P_9 only dropped. For P_2, P_5, P_7 and P_9, the amplitude of the pressure drop rate decreased successively and the duration time of the pressure drop became shorter with increasing distance from the orifice.

3.1.2 Phase transition

Fig. 7 plots the evolution of fluid properties on the pressure-temperature phase diagram for tests 1, 2 and 3. Upon rupture, the instantaneous pressure drop was accompanied by the formation of droplets which caused sharp temperature falls in each test. The high environment temperature made the droplets gasification rapidly and caused the pressure

rebound or stagnation. Due to the rapidity of this process it was not captured by the temperature thermocouples as their response time was too slow. In test 1 the overall temperature drop amplitude was not obvious due to the small orifice diameter. In test 2 the lowest temperatures recorded by T_{18} and T_{18d} were -16 °C and -26 °C respectively. The lowest temperatures at the top and bottom of the pipe at locations 7.4 m, 54.2 m and 62.1 m from the orifice were similar and fell to 23 °C, 22 °C and 21 °C respectively. As indicated by the recorded thermodynamic trajectories of tests 1 and 2, no phase change was observed in the overall release process, but the instantaneous phase transitions should appear at the beginning of the releases. In test 3, the lowest values of T_2, T_{2d}, T_4 and T_{4d} dropped to 3 °C, 0 °C, 5 °C and 2 °C when the pipeline pressure dropped to 1.56 MPa, and the lowest values of T_{16}, T_{16d}, T_{18} and T_{18d} fell to - 56 °C, -42 °C, -64 °C and -69 °C when the pipeline pressure dropped to 0.23 MPa, which suggested that the gaseous CO_2 at the pipeline end transformed to the gas-liquid phase in the last period of test 3.

3.2 Dense phase tests

3.2.1 Pressure response

Fig. 8 shows the pressure evolutions for tests 4, 5 and 6. The total depressurization times of each experiment were 7300 s, 482 s and 40 s respectively. As shown in Fig. 10(a) and (b), the depressurization process for tests 4 and 5 are very similar. For test 4 and test 5, during phase I of depressurization a sharp decline in pressure is observed for both tests, lasting about 34 s and 4.7 s respectively. During phase II of depressurization, the inventories achieve saturation pressure (P_S), initially at pressures of 5.08 MPa for test 4 and 5.02 MPa for test 5. Fluid pressures and temperatures then decline along the saturation line for duration times of circa

5838 s and 363 s respectively. When inventory properties reach the triple point pressure (P_T) the 3rd phase of depressurization begins, this 3rd phase lasts about 1428 s and 119 s respectively for tests 4 and 5.

As shown in the magnified regions of Fig. 8(a) and (b), the pressure drop processes of depressurization in phase I consisted of about 40 and 4 passes of the decompression wave for tests 4 and 5 respectively. With the propagation of decompression wave, the pressure fluctuation gradually weakened until it disappeared at the end of phase I. During the pressure response process of the 1st period of the dense tests there was an obvious slowdown between sharp decline and rapid rise in pressures compared to that seen in tests 1 to 3. Comparing the pressure response parameters of the 1st period of tests 4 and 5, ΔP_d of the two were similar, but ΔP_r of the former was higher than that of the later, and the P_{qs} of 9.04 MPa for test 4 was higher than the P_{qs} of 7.67 MPa for test 5.

As shown in Fig. 8(c) for test 6 (FBR), during phase I of depressurization, the pressure inside the pipeline sharply dropped to the saturation pressure, the rate of pressure loss then slowed down. During phase II of depressurization a significant pressure gradient was recorded along the length of the pipe. In phase III of depressurization the rate of pressure drop increased due to the formation of dry ice near the closed end of the pipe.

Fig. 9 shows the pressure change rate curve in 1st period of tests 4, 5 and 6. For tests 4 and 5, the minimum value of the pressure change rate decreased successively with increasing distance from the orifice. The maximum value of the pressure change rate at P_2 was much smaller than that at P_5, P_7 and P_9. For P_5, P_7 and P_9, the amplitude of the pressure rise rate was much larger than that of the pressure drop rate, but it's opposite at P_2. The wide

fluctuations of the pressure change rate were caused by bubble nucleation. For teat 6, the pressure change rate curve in the 1st phase was similar to that for test 3. However, the amplitude of the pressure drop rate along the pipe was much greater for test 6 than for test 3, while the duration time of the pressure drop of test 6 was shorter than that of test 3. This suggested that the bubble nucleation rate was much greater than the droplet gasification rate.

3.2.2 Phase transition

Fig. 10 shows the evolution of fluid pressure and temperature plotted on the CO_2 phase diagram for tests 4 to 6. Point A indicates the initial phase of each experiment, and the points B and C are the locations of phase changes. The low-response thermocouples couldn't captured the instantaneous temperature change after the rupture in tests 4 to 6, which was similar to that in the gaseous CO_2 releases. After the start of release, due to the low compressibility of dense CO_2 the pressure inside the pipeline fell rapidly to the saturation pressure i.e. from point A to B, corresponded to phase I of depressurization. The fluid temperature drop was not large as the dense (liquid) CO_2 couldn't release its heat fast enough. During phase II of depressurization the saturation properties evolve from points B to C. Due to the large release rate the measured temperature inside the pipeline tended to shift away from the saturation temperature, indicating the fluid was superheated. At point C, the inventory reached the CO_2 triple point pressure (0.52 MPa), the subsequent generation of the dry ice at the bottom of the pipeline made the flow phase change to gas-solid flow. For test 4, T_2, T_4, T_{16} and T_{18} started to deviate from the saturation line at the point B and T_{2d}, T_{4d}, T_{16d} and T_{18d} started to deviate from the saturation line at the point C .This result showed that the transition from gas-liquid phase CO_2 to gaseous CO_2 during phase II of depressurization

occurred first at the top of the pipe. The phase transition along the length of the pipeline was not significantly different during the small bore release. For test 5, recorded temperatures at T_2, T_4, T_9, T_{18}, T_{2d}, T_{4d}, T_{9d} and T_{18d} started to deviate from the saturation line when the respective pressures reached 4.96 MPa, 4.93 MPa, 4.90 MPa, 0.52 MPa, 1.42 MPa, 1.36 MPa, 1.01 MPa and 0.52 MPa. This result showed that the gas-liquid phase CO_2 near the orifice deviated from the saturation line and transformed into gas first, with the pressure in continuous decline eventually all the inventory in the pipe transformed into gaseous CO_2. CO_2 gas was observed at the top of the pipe first. For test 6, T_2, T_{2d}, T_4 and T_{4d} started to deviate from the saturation line when the pressure reached 0.69 MPa and T_{16}, T_{16d}, T_{18} and T_{18d} started to deviate from the saturation line when the pressure reached 0.10 MPa. This result showed that the phase transition at the top and bottom of the pipe was similar during the full bore release due to the large release rate. The lowest temperatures of test 4, test 5 and test 6 were -53 °C, -66 °C and -72 °C respectively. This result indicates that lower minimum temperatures in the overall release process are reached with larger orifice diameters.

4 Discussion

In order to simulate an actual CO_2 pipeline, a large-scale fully instrumented test pipeline with a total length of 258 m and an inner diameter of 233 mm was developed to study pressure responses and phase transitions of pure CO_2 pipeline blowdown. The dual-disc blasting device was designed to made the release device safe, controllable and being capable of transient release. Such a large capacity pipeline was essential as it permitted shock tube depressurization tests of long enough duration to enable the capture of sufficient data for analysis, but they were difficult and expensive to operate. In addition, given the highly

turbulent flows expected during the depressurization tests, a sufficiently large diameter pipe was required in order to avoid complications associated with fluid/wall frictional heating effects [26].

The mechanisms of pressure response were found in gaseous and dense CO_2 releases from a pipeline, as shown in Fig. 11. This process involved detailed consideration of several competing and often interacting factors including heat and mass transfer, unsteady fluid flow and thermodynamics [27]. The heat transfer effects during the release consisted of the conductive heat transfer within the pipe wall (H_1), the convective heat transfers between the flowing fluid and the pipe wall (H_2), between the outside ambient and the pipe wall (H_3), between the escaping fluid and the orifice (H_4), and within the flowing fluid (H_5). After the rupture, the pressure along the pipeline dropped quickly when the leading edge of decompression wave moved at the speed of sound at the initial conditions, then exponentially rebounded to a quasi-static level. The reasons of pressure rebound were the droplet generation and gasification for gas phase CO_2 and the bubble nucleation for dense phase CO_2 respectively. The process of pressure drop and rebound was accompanied by the occurrence of gas-liquid two-phase flow. The gas-liquid two-phase transformed into the gas phase for gaseous CO_2 depressurization process and the gas-liquid homogeneous phase for dense CO_2 releases respectively when the pressure rebound disappeared inside the pipe. The short duration time of pressure undershoot and rebound required the pressure sensors and the thermocouples with a higher frequency response and a higher accuracy for more reliable experimental results. The pressure sensors with a high-response frequency of 100 kHz could measure the pressure responses, but the thermocouples with a low-response time of 100 ms

didn't captured the instantaneous temperature change. Therefore, the instantaneous phase transitions at the beginning of the releases couldn't reflect on the pressure-temperature development plotted on the CO_2 phase diagram. However, the high-response thermocouples with a very thin probe were expensive and easily damaged as result of the strict experimental conditions. In spite of this, the low-response thermocouples didn't affect the analysis of the temperature development and the phase change in the whole process of CO_2 release.

The leakage in a CO_2 pipeline could escalate to a propagating fracture if the force acting on the defect overcomes the fracture toughness of the wall material. The fracture may be either in the ductile or brittle regime depending on the nature of the rupture. The rupture or puncture of a CO_2 pipeline results in a series of expansion waves which propagate into the disturbed fluid [16]. The accurate prediction of pressure response and phase transition following pipeline rupture are extremely important since this information dictates all the major consequences associated with such failure including fracture propagation and CO_2 dispersion. The precise experimental tracking of these expansion waves and their propagation as a function of time and distance along the pipeline are extremely valuable to the development of a rigorous multiphase outflow model for predicting CO_2 discharge rate and fluid state during pipeline failure.

The experimental data can also provide the variation characteristics of the decompression speeds during the release for the fracture control design, which usually are used as input to the two curve model (TCM) together with the fracture propagation speed. In addition, it can be observed from the experimental analysis that the waveforms of the pressure response and the pressure change rate in gaseous and dense CO_2 releases are significantly different due to

the different orifice diameters used. In the real-time monitoring of a CO_2 pipeline, the leakage location and the leakage diameter size can be determined by the waveform characteristics of the pressure response and the pressure change rate.

5 Conclusions

This article has presented the results of an experimental study of pressure response and phase transition during pure CO_2 pipeline blowdown. Experiments were conducted using CO_2 in initially gaseous and dense phases with three different orifice sizes (15 mm, 50 mm and FBR) for a total of six experiments. From this experimental study selected conclusions are presented as follows:

(1) In all experiments the rapid expansion of the high pressure CO_2 at the orifice resulted in a decompression wave which propagated from the orifice to the closed pipeline end, where it subsequently reflected. Passage of the decompression wave through the inventory caused the pressure undershoot, rebound or slowdown successively, before quasi static pressures were achieved. Moreover, the nearer to the orifice the longer the quasi static pressure level was maintained.

(2) In the gaseous CO_2 releases, the pressure fall, rebound or slowdown was accompanied by droplet formation and rapid gasification. During the depressurization process, the CO_2 phase was generally gaseous near the orifice. When the release diameter was increased, the recorded variation in inventory pressure and temperature would closely follow the saturation line, the gas-liquid CO_2 would appear near the pipe end and the lowest temperature of the CO_2 at the bottom of the pipe was lower than that at the top.

(3) In the dense CO_2 releases, the pressure undershoot, rebound or slowdown occurred as the dense phase CO_2 transformed into a gas-liquid CO_2 mixture. With larger orifice diameters, a greater proportion of inventory in the pipeline remained in the saturation state and the lowest temperature achieved in the overall release process was lower. When the pressure fell to the CO_2 triple point, the CO_2 phase was mainly gas-solid with dry ice forming at the bottom of the pipeline.

Acknowledgement

The authors would like to acknowledge the funding received from the European Union Seventh Framework Programmes FP7-ENERGY-2009-1 under grant agreement number 241346 and FP7-ENERGY-2012-1STAGE under Grant agreement 309102.

References

[1] IPCC. Climate Change 2007: Mitigation of Climate Change. Contribution of Working Group III to the Fourth. Assessment Report of the Intergovernmental Panel on Climate Change 2007.

[2] Haszeldine RS. Carbon Capture and Storage: How Green Can Black Be? Nature 2009; 325:1647-1652.

[3] Chong FK, Lawrence KK, Lim PP, Poon MCY, Foo DCY, Lam HL, Tan RR PP. Planning of carbon capture storage deployment using process graph approach. Energy 2014; 76:641-651.

[4] IEA. Energy Technology Perspectives 2012: Pathways to a Clean Energy System 2012.

[5] Iribarren D, Petrakopoulou F, Dufour J. Environmental and thermodynamic evaluation of CO2 capture, transport and storage with and without enhanced resource recovery. Energy 2013; 50:477-85.

[6] Duncan IJ, Wang H. Estimating the likelihood of pipeline failure in CO_2 transmission pipelines: New insights on risks of carbon capture and storage. Int J Greenh Gas Con 2014; 21: 49-60.

[7] Mahgerefteh H, Brown S, Denton G. Modelling the impact of stream impurities on ductile fractures in CO_2 pipelines. Chemical Engineering Science 2012; 74:200-210.

[8] Molag M, Dam C. Modelling of accidental releases from a high pressure CO_2 pipelines. Energy Procedia 2011; 4:2301-2307.

[9] Lund H, Flatten T, Munkejord ST. Depressurization of carbon dioxide in pipelines – models and methods. Energy Procedia 2011; 4:2984-2991.

[10] Aursand E, Aursand P, Berstad T, Dørum C, Hammer M, Munkejord ST, Nordhagen HO. CO_2 pipeline integrity: A coupled fluid-structure model using a reference equation of state for CO_2. Energy Procedia 2013; 37:3113-3122.

[11] Martynov S, Brown S, Mahgerefteh H, Sundara V. Modelling choked flow for CO_2 from the dense phase to below the triple point. Int J Greenh Gas Con 2013; 19:552-558.

[12] Brown S, Martynov S, Mahgerefteh H, Chen SY, Zhang YC. Modelling the non-equilibrium two-phase flow during depressurisation of CO_2 pipelines. Int J Greenh Gas Con 2014; 30:9-18.

[13] Woolley RM, Fairweather M, Wareing CJ, Falle SAEG, Mahgerefteh H, Martynov S, Brown S, Narasimhamurthy VD, Storvik IE, Sælen L, Skjold T, Economou IG,

Tsangaris DM, Boulougouris GC, Diamantonis N, Cusco L, Wardman M, Gant SE, Wilday J, Zhang YC, Chen SY, Proust C, Hebrard J and Jamois D. CO_2PipeHaz: quantitative hazard assessment for next generation CO_2 pipelines. Energy Procedia 2014, 63:2510–2529.

[14] Botros KK, Hippert E Jr, Craidy P. Measuring decompression wave speed in CO_2 mixtures by a shock tube. Pipelines International 2013; 16:22-28.

[15] Woolley RM, Fairweather M, Wareing CJ, Proust C, Hebrard J, Jamois D, Narasimhamurthy V D, Storvik IE, Skjold T, Falle SAEG, Brown S, Mahgerefteh H, Martynov S, Gant SE, Tsangaris D M, Economou IG, Boulougouris GC, Diamantonis NI. An integrated, multi-scale modelling approach for the simulation of multiphase dispersion from accidental CO_2 pipeline releases in realistic terrain. Int J Greenh Gas Con 2014; 27:221-238.

[16] Mahgerefteh H, Zhang P, Brown S. Modelling brittle fracture propagation in gas and dense-phase CO2 transportation pipelines. Int J Greenh Gas Con 2016; 46: 39-47.

[17] Cosham A, Jones DG, Armstrong K, Allason D, Barnett J. Ruptures in gas pipelines, liquid pipelines and dense phase carbon dioxide pipelines. Proceedings of the 2012 9th International Pipeline Conference; 2012.

[18] Clausen S, Oosterkamp A, Strøm KL. Depressurization of a 50 km long 24 inches CO_2 pipeline. Energy Procedia 2012; 23:256–265.

[19] Cosham A, Jones DG, Armstrong K, Allason D, Barnett J. The depressurization behaviour of carbon dioxide in the dense phase. Proceedings of the 2012 9th International Pipeline Conference; 2012.

[20] Li K, Zhou XJ, Tu R, Xie QY, Jiang X. The flow and heat transfer characteristics of supercritical CO_2 leakage from a pipeline. Energy 2014; 71:665-672.

[21] Huh C, Cho MI, Hong S, Kang SG. Effect of Impurities on depressurization of CO_2 pipeline transport. Energy Procedia 2014; 63:2583–2588.

[22] Koeijera Gd, Borch JH, Jakobsenb J, Drescher M. Experiments and modeling of two-phase transient flow during CO_2 pipeline depressurization. Energy Procedia 2009; 1:1683-1689.

[23] Drescher M, Varholm K, Munkejord ST, Hammer M, Held R, Koeijer Gd, Barnett J. Experiments and modelling of two-phase transient flow during pipeline depressurization of CO_2 with various N_2 compositions. Energy Procedia 2014; 63:2448-2457.

[24] Vree B, Ahmad M, Buit L, Florisson O. Rapid depressurization of a CO_2 pipeline – an experimental study. Int J Greenh Gas Con 2015; 41:41–49

[25] Ahmad M, Lowesmith B, Koeijer Gd, Nilsen S, Tonda H, Spinelli C, Cooper R, Clausen S, Mendes R, Florisson O. COSHER joint industry project: Large scale pipeline rupture tests to study CO_2 release and dispersion. Int J Greenh Gas Con 2015; 37: 340–353.

[26] Mahgerefteh H, Oke A, Rykov Y. Efficient numerical solution for highly transient flows. Chem Eng Sci 2006a; 61(15): 5049-5056.

[27] Mahgerefteh H, Atti O. Modeling low-temperature-induced failure of pressurized pipelines. AIChE J 2006; 52(3): 1248-1257.

Figures

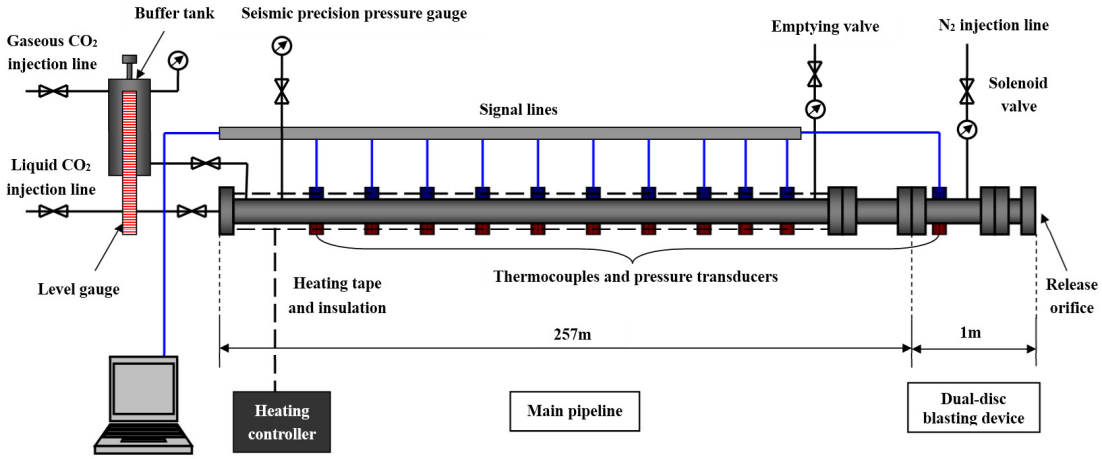

(a) Schematic diagram

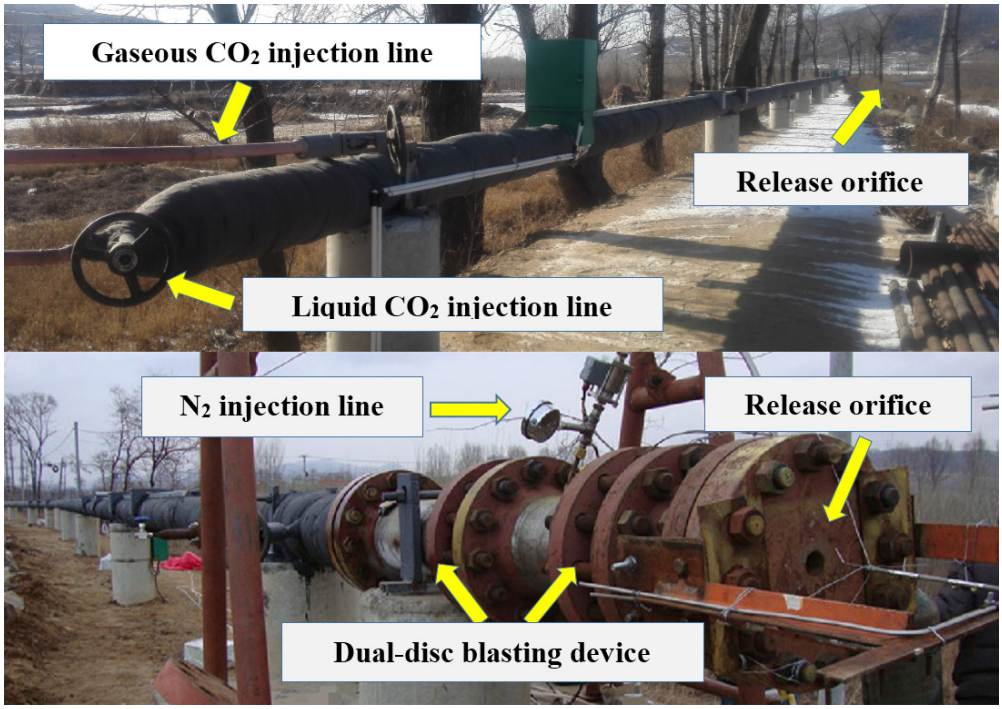

(b) Photograph

Fig. 1 Schematic and scene graph of experimental apparatus.

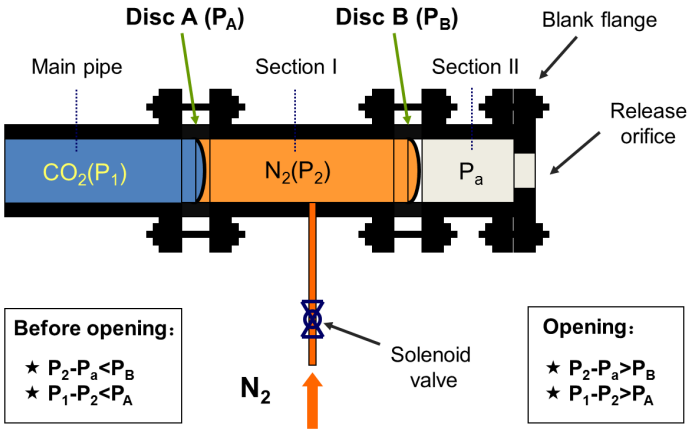

Fig. 2 Schematic of dual-disc blasting device.

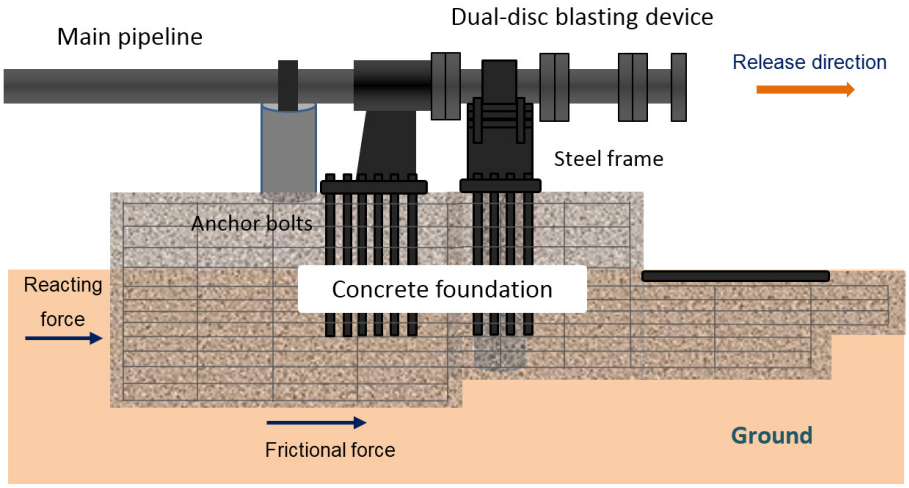

(a) Schematic diagram

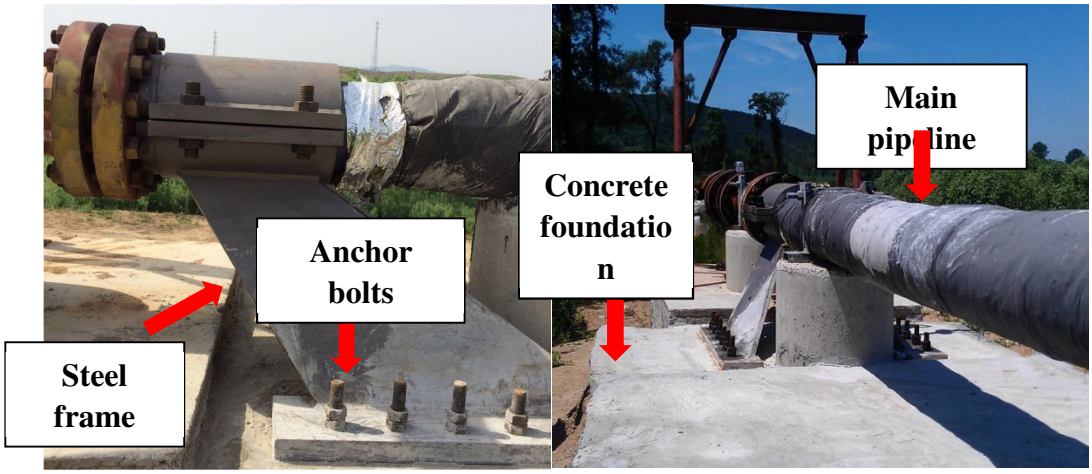

(b) Photograph

Fig. 3 Illustration of the reinforcing device.

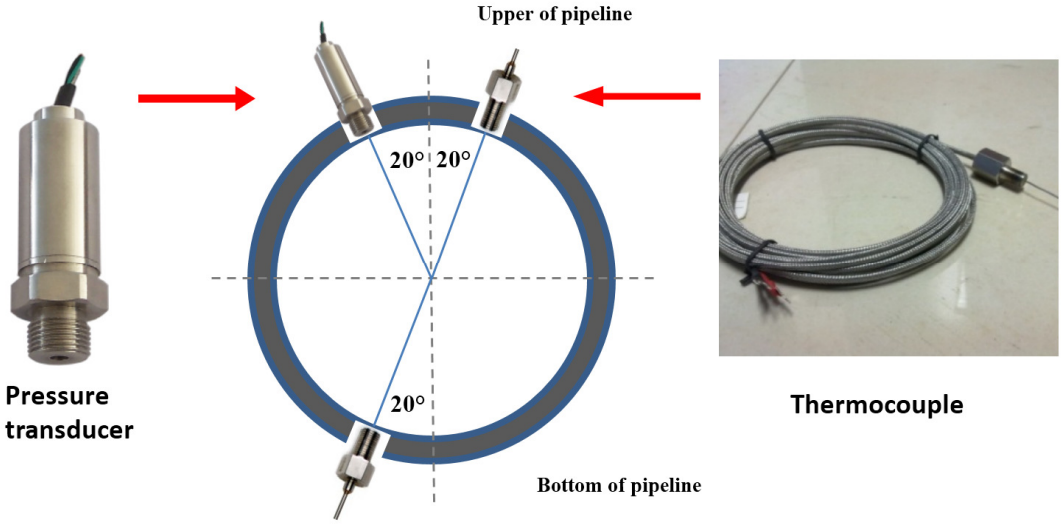

Fig. 4 Measurement point locations.

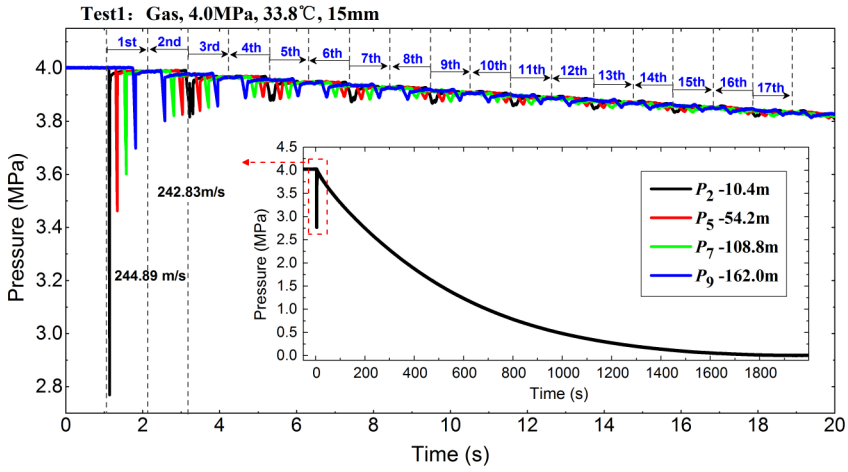

(a) Test1-15 mm orifice

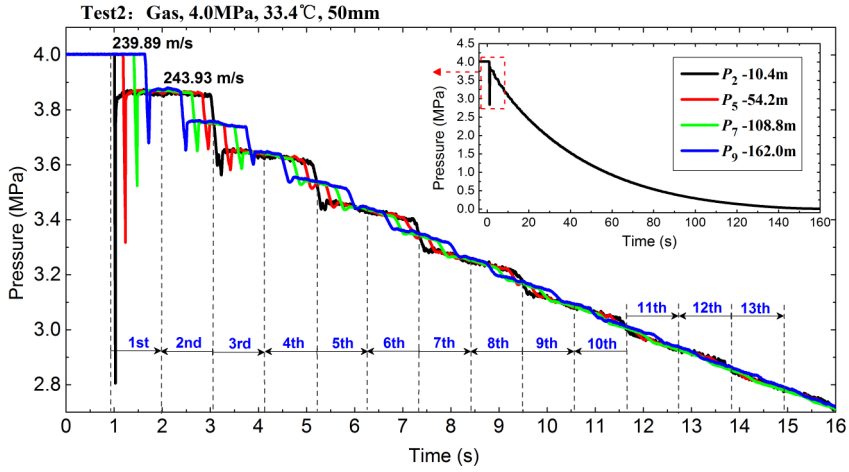

(b) Test2-50 mm orifice

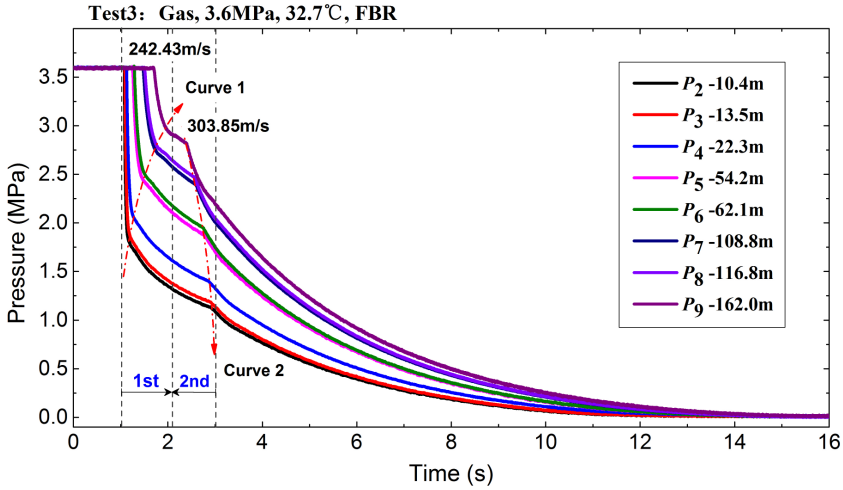

(c) Test3-FBR

Fig. 5 Pressure evolutions of the gaseous CO_2 release experiments with three different orifices (15 mm, 50 mm and FBR).

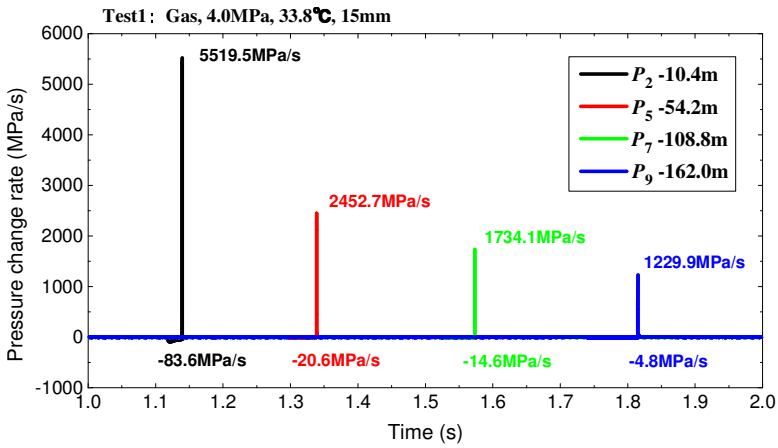

(a) Test1-15 mm orifice

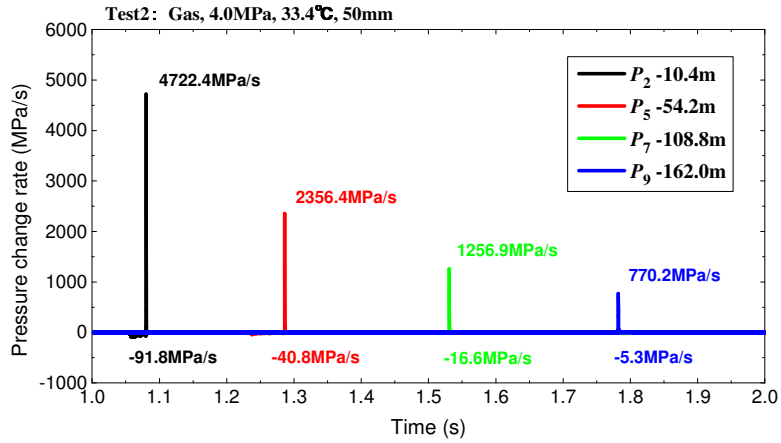

(b) Test2-50 mm orifice

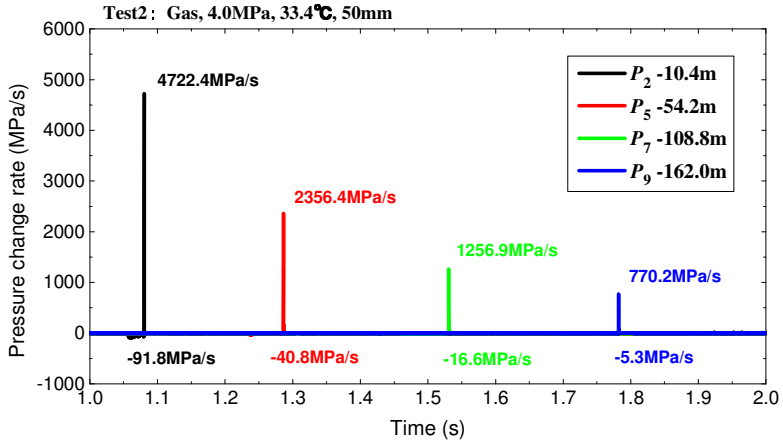

(c) Test3-FBR

Fig. 6 Pressure change rate curve in 1st phase of the gaseous CO_2 release experiments with three different orifices (15 mm, 50 mm and FBR).

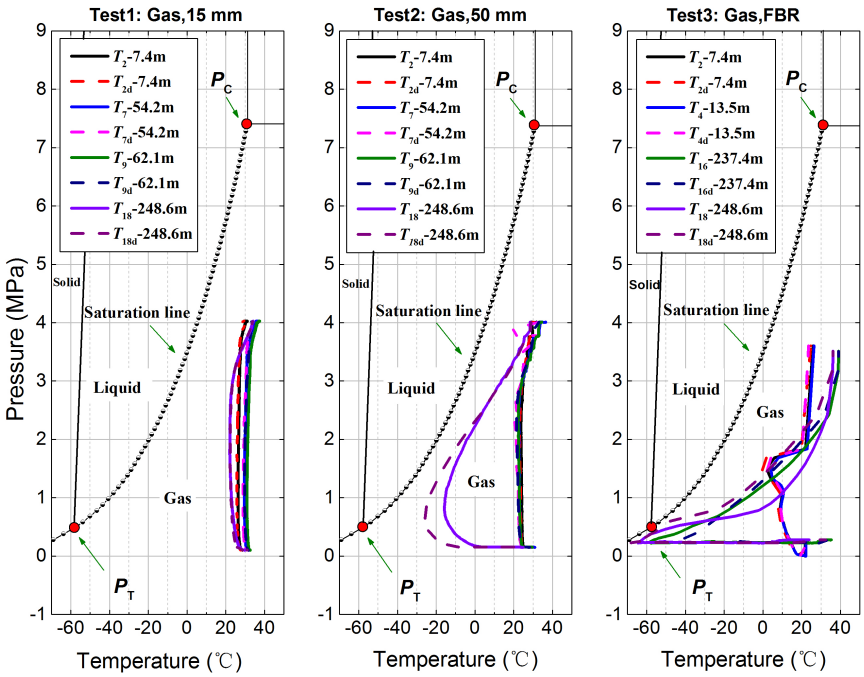

Fig. 7 Pressure-temperature development with three gaseous CO_2 release experiments.

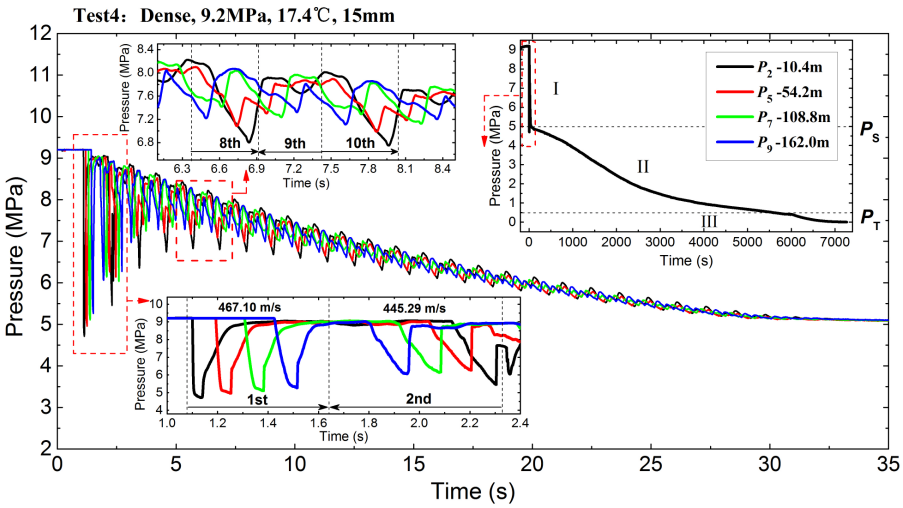

(a) Test4-15 mm orifice

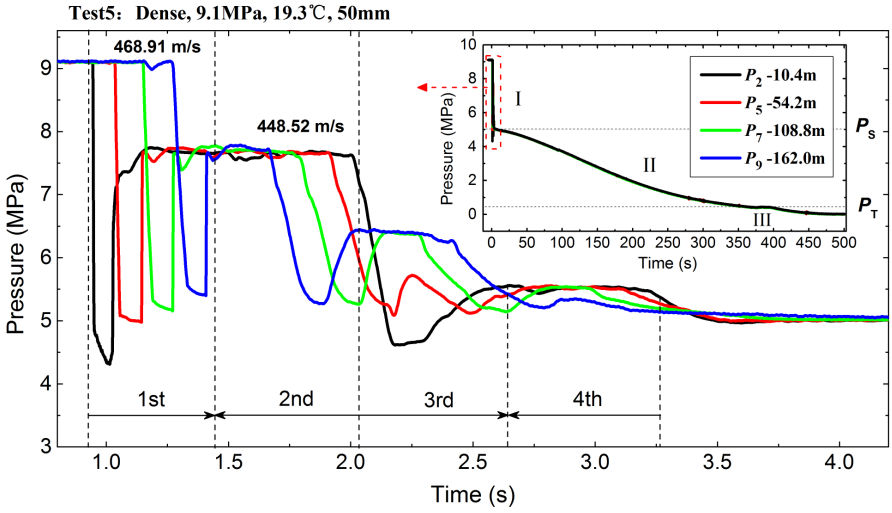

(b) Test5-50 mm orifice

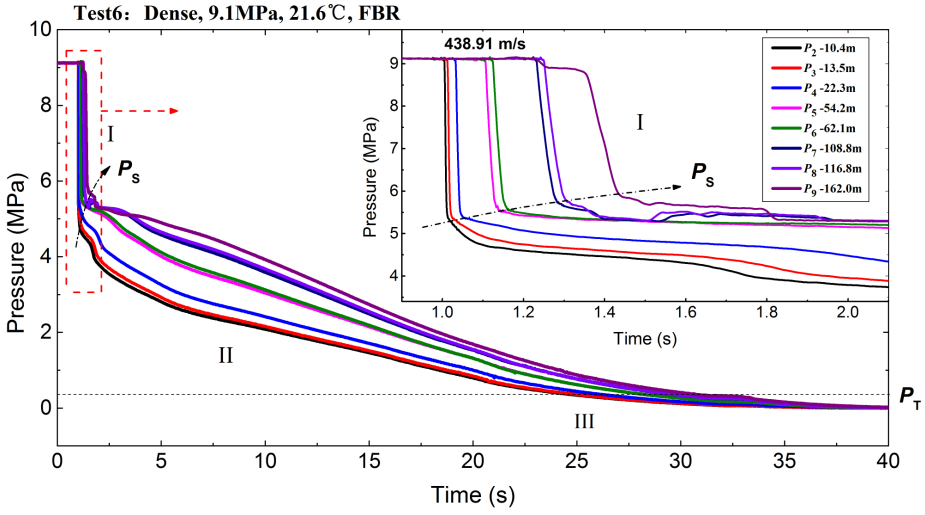

(c) Test6-FBR

Fig. 8 Pressure evolutions of the dense CO_2 release experiments with three different orifices (15 mm, 50 mm and FBR).

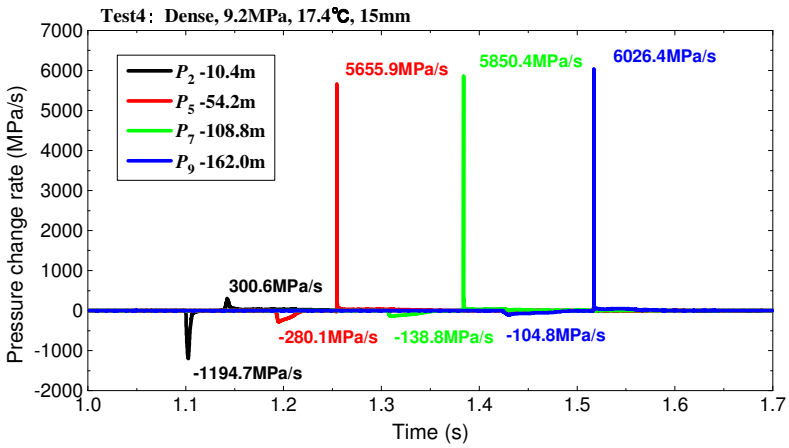

(a) Test1-15 mm orifice

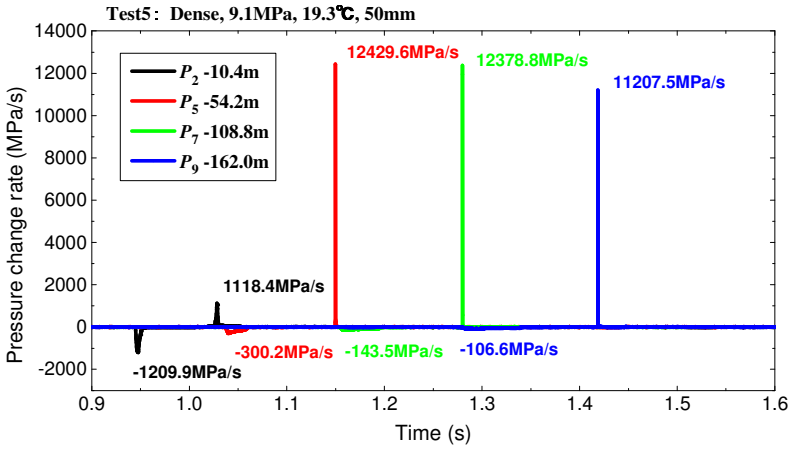

(b) Test2-50 mm orifice

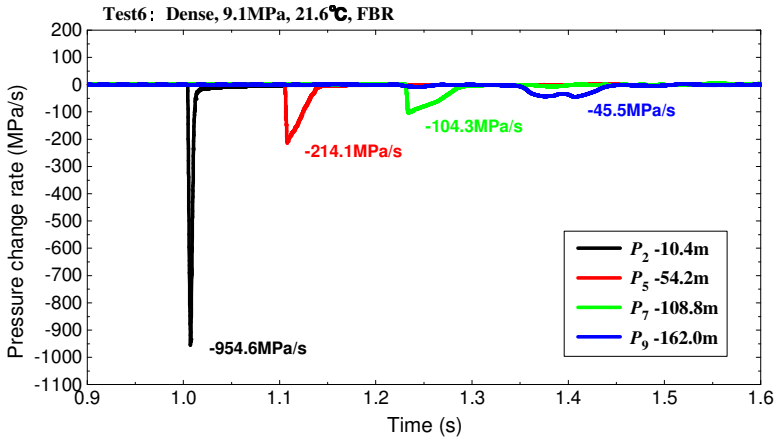

(c) Test6-FBR

Fig. 9 Pressure change rate curve in 1st phase of the dense CO_2 release experiments with three different orifices (15 mm, 50 mm and FBR).

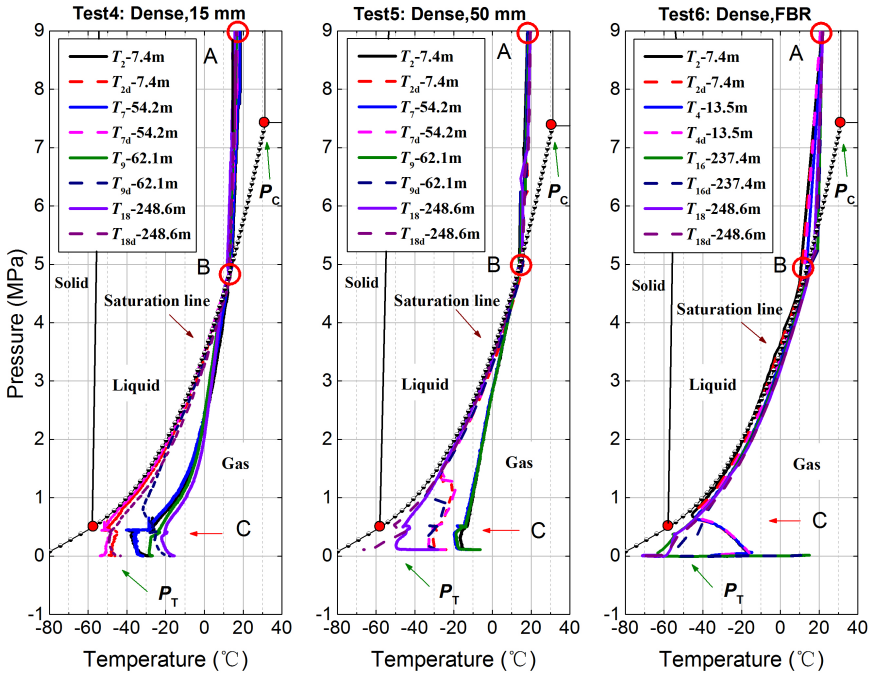

Fig. 10 Pressure-temperature development with three dense CO_2 release experiments.

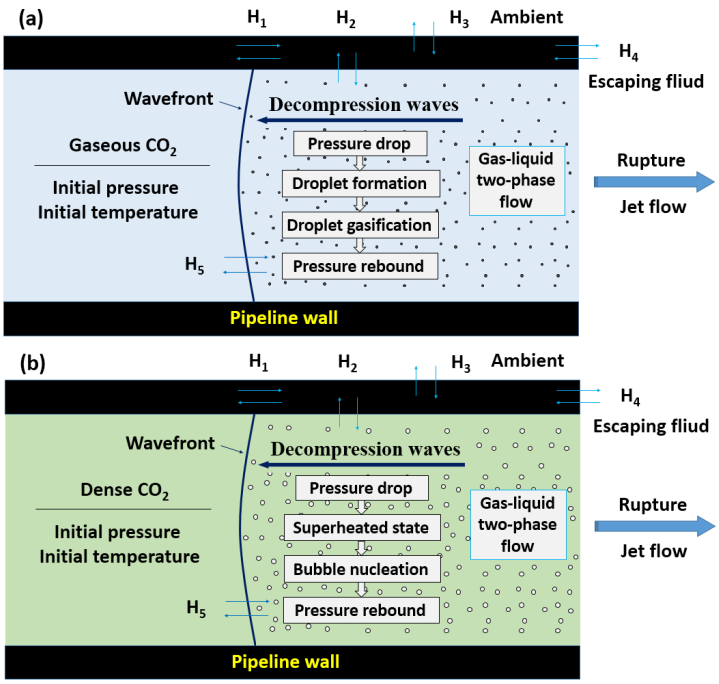

Fig. 11 Schematic of pressure response process in gaseous and dense CO_2 releases.